Distance Estimation and Material Classification of a Compliant Tactile Sensor Using Vibration Modes and Support Vector Machine

S. R. GUNASEKARA[1], H. N. T. K. KALDERA[2], N. HARISCHANDRA[3], L. SAMARANAYAKE[4]

Department of Electrical and Electronic Engineering, University of Peradeniya, Sri Lanka

(1.*shanakag@eng.pdn.ac.lk*, 2.*nikalal.k@eng.pdn.ac.lk*, 3.*nalin@ee.pdn.ac.lk*, 4.*lilantha@ee.pdn.ac.lk*)

Abstract: Many animals possess actively movable tactile sensors in their heads, to explore the near-range space. During locomotion, an antenna is used in near range orientation, for example, in detecting, localizing, probing, and negotiating obstacles. A bionic tactile sensor used in the present work was inspired by the antenna of the stick insects. The sensor is able to detect an obstacle and its location in 3D (Three dimensional) space. The vibration signals are analyzed in the frequency domain using Fast Fourier Transform (FFT) to estimate the distances. Signal processing algorithms, Artificial Neural Network (ANN) and Support Vector Machine (SVM) are used for the analysis and prediction processes. These three prediction techniques are compared for both distance estimation and material classification processes. When estimating the distances, the accuracy of estimation is deteriorated towards the tip of the probe due to the change in the vibration modes. Since the vibration data within that region have high a variance, the accuracy in distance estimation and material classification are lower towards the tip. The change in vibration mode is mathematically analyzed and a solution is proposed to estimate the distance along the full range of the probe.

Key words: Vibration based active tactile sensor, Artificial Neural Network, Support vector machines, Distance estimation, Vibration modes, Euler-Bernoulli beam element.

1 Introduction

Walking animals are fully autonomous creatures of the nature and are highly adaptive in object detection and localization using their sensitive sensors. Tactile sensors are used as near range sensing elements by most animals, and the information through physical interaction with their near range environment is measured (Dürr, et al., 2007).

Many animals like rats and cats use active whisker movements to detect and scan objects in the vicinity of the body, and insects like honey bee (*Apis mellifera*) and crustaceans use antenna for obstacle localization, orientation and pattern recognition (Krause, et al., 2014). Unlike vision, direct tactile sampling of an object allows feeling of object properties such as chemical properties, temperature, texture, and humidity. In most cases, these properties provide important measurements, and they are hard to identify using intangible sensors. Since the tactile sensor used here does not depend on lighting conditions, it works under any lighting conditions and the readings will not be affected by the light intensity. It is useful to analyze the properties of tactile sensors and apply them in robotics, just as they play a major role in the animal kingdom.

In the present paper, a bionic active tactile sensor inspired by the antenna of the Indian stick insect, *Carausius morosus* is used (Dürr, et al., 2007; Hoinville, et al., 2014). It consists of an acceleration sensor mounted on the tip of the probe, which is capable of near-range tactile localization and predicting the contact distances up to an accuracy level of 0.5 cm, using an ANN (Hoinville, et al., 2014). The contact distance is mainly determined by using the dominant frequency of the damped oscillations of the probe, and the damping properties are used for material classification The existing methods are able to estimate the contact distances and material classifica-

tion along 75% of the probe length, where one half of the problematic range contains the most distal sites (Dürr, et al., 2007; Patanè, et al., 2012). A detailed discussion of the reasons behind this abnormal behavior of the vibration pattern of the final quarter of the antenna is not found in the literature.

The initial study of the present work has focused on identifying the possible causes for the changes of the vibration patterns of the final quarter of the antenna, by using mathematical analysis based on the Euler-Bernoulli beam element model of the antenna probe. During this analysis, a suitable method to use the full range of the antenna probe is suggested. Even though the Artificial Neural Network (ANN) is a powerful machine learning approach, it has many drawbacks; for example, there is no standard method to determine and optimize the structure of the network and also ANNs are computationally expensive for training and testing. In the present work, ANNs are used for comparison purposes as they have been used in other studies (Hellbach, et al., 2010; Patanè, et al., 2012). Another machine learning technique called Support Vector Machines (SVM), which can give solutions to most of the mentioned drawbacks (Bisgin, et al., 2018; Ren, 2012) is used as the primary approach. A comparison between the results, observed from ANN, SVM and basic signal processing algorithms, are presented.

2 Methodology

The active tactile sensor consists of an acrylic fiber antenna probe with an accelerometer that is mounted on the tip of the antenna.

2.1 Distance Estimation

The typical acceleration sensor provides acceleration readings of the tip of the antenna, in two orthogonal directions X and Z. The second norm of the X and Z components is taken as the total acceleration of the antenna tip:

$$\text{Resultant Acceleration} = \sqrt{X^2 + Z^2} \quad (1)$$

The vibration pattern of the antenna tip at a distance 17 cm from the hinge point of a brass rod is shown in Fig.1.

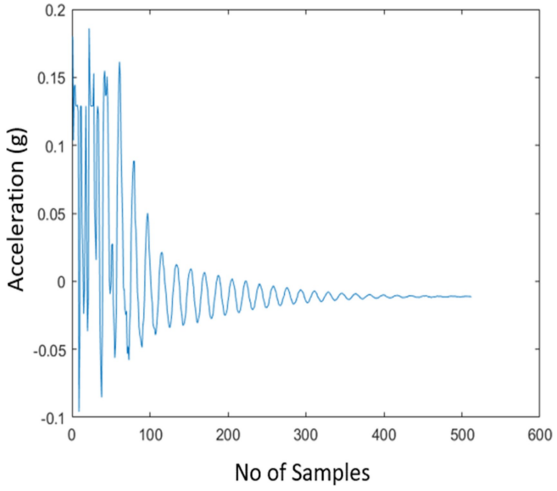

Fig. 1 Vibration signal using MPU6050 sensor when object was at 17cm away from the hinge point.

According to previous research in this area (Dürr, et al., 2007; Patanè, et al., 2012) it is difficult to identify the small consecutive distances by using time domain techniques. Therefore, in the present work, frequency domain techniques are used to estimate the contact distances from the hinge point (Volker, no date). The time domain signals of the X and Z axis are converted to the frequency domain by taking their FFT and the norm is calculated according to (1). The norm of the two FFT spectrums is shown in Fig.2. The dominant frequency component of the FFT spectrum is identified as the feature to estimate the contact location (Patanè, et al., 2012; Harischandra & Dürr, 2012). Initially, the antenna length is taken as 40 cm and a data set is collected for five different materials (Aluminum, Brass, Wood, Steel and PVC) as the objects. The dominant frequency method is applied to all the data, collected using the five materials. Although a linear variation has been observed initially, a deviation from the linear variation is observed at 29.5 cm away from the hinge point. Therefore, the data set is statistically analyzed, providing the standard deviation and the variance. The variation of the standard deviation and the variance is shown in Fig.3. According to the box plot graph in Fig.3, a high variation of the

dominant frequency near 30 cm is observed. This variation may be due to reasons such as the contact point might be near a changing point of the vibration mode, more noise may enter the readings due to the contact point being very close to the sensor, and the limitations in the sampling frequency. For further investigation, the antenna probe length is increased to 50cm from 40cm, and the same procedure is followed. In this situation also, a similar variation occurs at 39.5cm away from the hinge point.

2.2 Mathematical Analysis of the Probe

Beam members are widely used the basic structural components in mechanical, aeronautical, automobile and civil engineering fields. Therefore, efforts have gone into their static and dynamic analyses. In the Bernoulli-Euler theory, the shear deformation due to bending is neglected (De Silva, 2007) in the formulation of the spectral and finite element methods (Hamioud & Khalfallah, 2016).

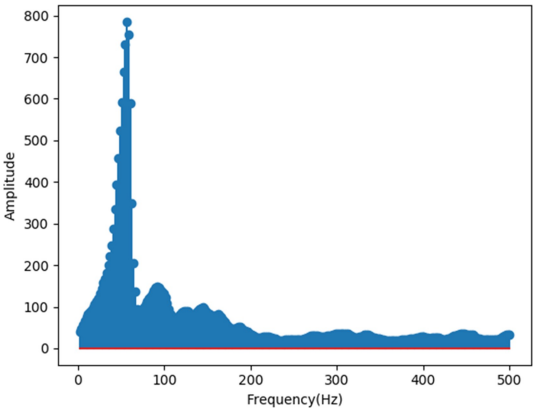

Fig. 2 FFT norm spectrum 17cm away from the hinge point.

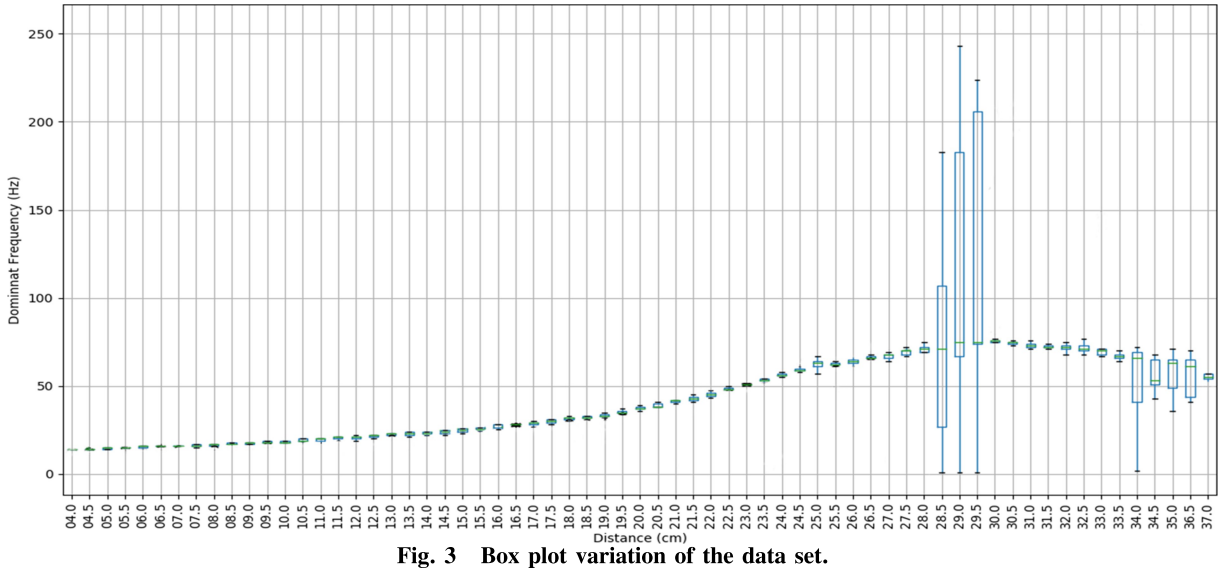

Fig. 3 Box plot variation of the data set.

With the aim of analyzing the variation beyond 80 % length of the probe, a vibration modal analysis is carried out. The probe is numerically modelled using planer Euler-Bernoulli (E-B) beam elements. An E-B beam element has two nodes per element and each node has two degrees of freedom (DOF), as shown in Fig 4. These degrees of freedom are arranged as $[\ v_1\ ,\ v_2\ ,\ \theta_1\ ,\ \theta_2\ ]$, where v_1, v_2 are the translational DOFs and θ_1, θ_2 are the rotational DOFs. With respect to the 2D (two dimensional) global coordinates system, the stiffness matrix of the E-B beam element is given by the matrix K and the consistent mass matrix of the E-B beam element is given by matrix M [8]:

$$K = \frac{EI}{l^3}\begin{pmatrix} 12 & 6l & -12 & 6l \\ 6l & 4l^2 & -6l & 2l^2 \\ -12 & -6l & 12 & 6l \\ 6l & 2l^2 & -6l & 4l^2 \end{pmatrix}$$

$$M=\frac{\rho Al}{420}\begin{pmatrix}156 & 22l & 54 & -13l\\ 22l & 4l^2 & 13l & -3l^2\\ 54 & 13l & 156 & -22l\\ -13l & -3l^2 & -22l & 4l^2\end{pmatrix}$$

where,

E = Young's modulus of the material (N/m^2)

I = moment of inertia of the beam (kg/m^2)

L = length of the beam (m)

ρ = mass density of the beam (kg/m^3)

A = area of the cross section (m^2)

The associated eigenvalue problem is (De Silva, 2007)

$$[K-\omega^2 M][\varnothing]=[0] \quad (2)$$

where,

ω = natural frequencies of the beam

$\varnothing$ = mode shape vectors

Two frequencies of the vibration modes are obtained for nontrivial solution of (2), given by, det ($|K-\omega^2 M|$) = 0. By substituting the resulting two ω values into (2), the vibration mode shapes of the structure can be obtained from the eigenvector $\varnothing$.

The antenna probe used here is modeled with two E-B elements, as shown in Fig.5. Since the antenna probe is in the horizontal plane, element local coordinate and global coordinate systems coincide, and the rotational transformation matrix becomes the identity matrix. If the local and global coordinate systems do not coincide, K and M should be multiplied with a rotational transformation matrix. As the antenna probe model has two E-B elements, in order to get the structural stiffness matrix K1 and the structural mass matrix M1, the K and M matrices of both elements should be assembled.

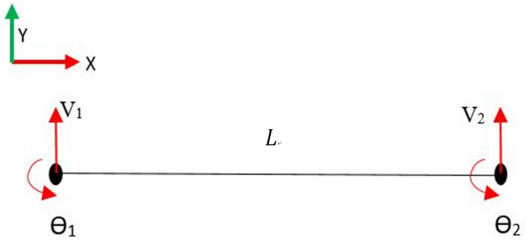

Fig. 4 Euler-Bernoulli beam element.

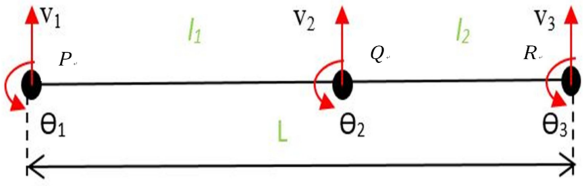

Fig. 5 The structural model of the antenna probe.

$$K_1=\frac{EI}{l^3}\begin{pmatrix}12 & 6l_1 & -12 & 6l_1 & 0 & 0\\ 6l_1 & 4l^2 & -6l & 2l^2 & 0 & 0\\ -12 & -6l_1 & 24 & 6(l_2-l_1) & -12 & 6l_2\\ -12 & -6l_1 & 6(l_2-l_1) & 4(l_1^2+l_2^2) & -6l^2 & 2l_2^2\\ 0 & 0 & -12 & 6l_2 & 12 & -6l_2\\ 0 & 0 & 6l_2 & 2l_2^2 & -6l_2 & 4l_2^2\end{pmatrix}$$

$$M_1=\frac{\rho Al}{420}\begin{pmatrix}156 & 22l_1 & 54 & -13l_1 & 0 & 0\\ 22l_1 & 4l_1^2 & 13l_1 & -3l_1^2 & 0 & 0\\ 54 & 13l_1 & 312 & 22(l_2-l_1) & 54 & -13l_2\\ -13l_1 & -13l_1^2 & 22(l_2-l_1) & 4(l_1^2+l_2^2) & 13l_2 & -3l_2^2\\ 0 & 0 & 54 & 13l_2 & 156 & -22l_2\\ 0 & 0 & -13l_1 & -3l_1^2 & -22l_2 & 4l_2^2\end{pmatrix}$$

where,

v_1, v_2, v_3 = translational DOF

θ_1, θ_2, θ_3 = rotational DOF

l_1 = length of 1st E-B element

l_2 = length of 2nd E-B element

P = hinge point

Q = object's contact point

R = free end

After combining the matrices K and M, (2) is modified as,

$$[\mathrm{K1} - \omega^2\ \mathrm{M1}][\varnothing] = [0] \qquad (3)$$

The most flexible mode is the dominant mode and its frequency is considered as the dominant frequency of the structure. Vibration modes at every contact point could be obtained by changing the values of l_1 and l_2. By taking l_1 as $0.25L$, $0.5L$, $0.75L$, $0.8L$, and $0.9L$, the system is solved numerically. Then the mode shapes are obtained using the eigenvectors $\varnothing$, and most flexible mode shape is analyzed. As the verification process of the mathematical analysis, the vibration signal is analyzed using wavelet transform. Since the FFT failed to give time resolution of the signal, it is impossible to identify the mode of vibration changes in the antenna element using the FFT. But the wavelet transform is able to provide a clear idea about time and frequency. Therefore the norm vibration signal of the antenna beam is analyzed using wavelet transform at the same distances as those used in the numerical analysis. Then it can clearly verify the mode changes of the antenna beam.

2.3 Material Classification

Apart from the distance measurements, the sensor feelers are able to classify the properties of the contact object (Hellbach, et al., 2010; Patanè, et al., 2012). Tactile sensor reads the acceleration data after a small impact with the object material, and the antenna gives energy to the contact object. According to energy conservation, the given energy should be absorbed by the antenna itself and transferred to the contact object. Since the amount of absorbed energy depends on the contact object's material properties, the rest of the energy is absorbed by the antenna probe, and should depend on the material (law of energy conservation) of contact objects. Since the surrounding environment remains constant, the performance of the damping time depends only on the characteristics of the contact material.

Using this concept, the damping time for five different materials are calculated. The time domain norm signal of the X and Z axes is taken for the material classification process up to 80% length of the antenna. As the vibration signal contains noise, it is pre-filtered using a Chebyshev second order band pass filter. After that, a damping time constant is calculated by fitting a general exponential model to the vibration signal using MATLAB signal processing toolbox:

$$F(x) = a\, e^{bx} \qquad (4)$$

where $\tau = 1/b$ is the time constant and a is the gain.

Since vibration details for 25 contacts are taken for all contact distances, 25 time constants are calculated for one contact distance, and they are averaged.

2.4 Classification Techniques

2.4.1 Artificial Neural Network (ANN)

AnArtificial Neural network (ANN) is a computational model that is inspired by the biological neural network in the human brain. The feed forward neural network was the first and the simplest type of ANN (Karray and de Silva, 2004). It consists of multiple neurons arranged in layers. Nodes from adjacent layers have connections or edges between them. These connections have weights associated with them. A multilayer perceptron (MLP) is a collection of multiple hidden layers apart from the input and output layer. With the help of nonlinear activation functions like sigmoid and tanh, an MLP is able to build a nonlinear relationship between the features and the target, for either classification or regression. The ANN has many advantages; for example, after ANN training, the data may produce useful outputs even with incomplete information; parallel processing capabilities; and learning events and making decisions by commenting on similar events. It has some significant drawbacks as well; for example, inadequate theoretical backing; back-propagation usually converges only to locally optimal solutions; and the behavior of the network cannot be explained after the model is created. Despite the drawbacks, it is used

here to benchmark the classification process.

2.4.2 Support Vector Machine (SVM)

A Support Vector Machine (SVM) is a supervised machine learning technique, and is applicable in both classification and regression problems. The algorithm used in the SVM creates a hyperplane in high dimensional space, which separates the classes in a classification problem. The separating hyperplane is optimized by maximizing the distance of either class to the separating hyperplane and minimizing the risk of misclassifying the training samples and unseen test samples. The kernel methods consist of a kernel function. These functions map the nonlinear separable input space into a higher dimensional linear separable feature space. In the new higher dimensional linear separable feature space, SVM can perform as a general SVM. In SVM regression, the input data set is first mapped onto an *m*-dimensional feature space using a fixed (nonlinear) mapping, and then a linear model is constructed in this feature space. SVM is able to find the optimal separation hyperplane, and therefore the accuracy of this model is higher than with other classification models like ANN and K-means. Also, it can deal with very high dimensional data.

3 Experimental Verification

Antenna probe should bea structure, similar to a beam, that is vibration sensitive and compliant but also sufficiently stiff to maintain its shape during self-vibration, The antenna beam should be sufficiently soft, so as not to damage the obstacle, as a small impact is given to the obstacle while detecting the obstacles and collecting data (Patanè, et al., 2012). To achieve these properties, an acrylic fiber tube of 0.8 cm outer diameter, 0.6 cm inner diameter, and 40 cm length is selected as the antenna tube (Sayed, 2015).

An accelerometer (MPU6050) is mounted at the tip of the antenna to collect the vibration data. Since the Y axis is along the antenna axis itself, it does not provide any significant data. Therefore, only the X axis and the Z axis data are used in the calculations. A Raspberry Pi^{TM3} control board is used as the brain of the system and Python 3.0 is used as the programming language. The maximum sensitivity of the sensor is +/- 16g (g = 9.81 ms-2), and I2C communication protocol is used to communicate with the Raspberry Pi 3 microcontroller board (ElectronicWings, 2018). The sampling frequency of the data acquisition is set as 1 kHz to capture all frequencies of vibration up to 512 Hz. Since the maximum data transferring rate of the sensor via I^2C is 400 kHz, it is easy to achieve this sampling rate. A Kalman filter is used to filter out the noise in the vibration signal from the sensor (De Silva, 2017).

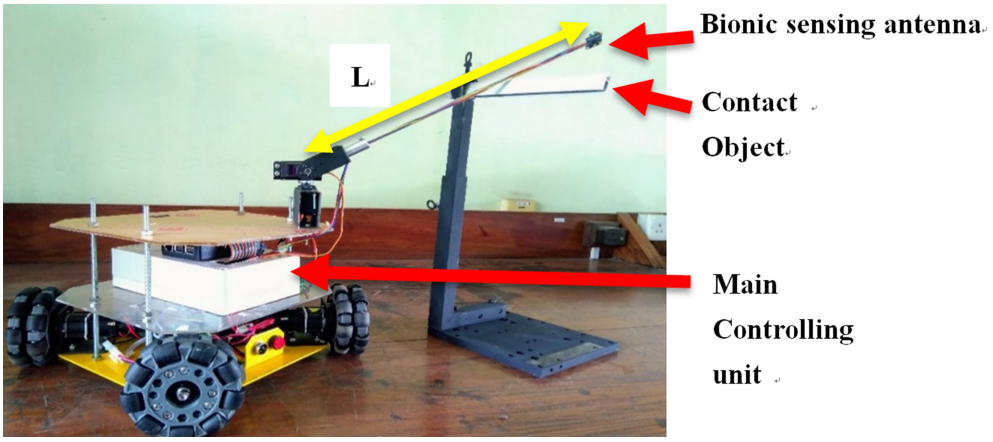

Fig. 6 The hardware setup: Basic module placement of the hardware, L indicate the distance measure from the hinge point.

The antenna probe is mounted on a pan-tilt unit. The following specifications have been considered in designing the pan-tilt unit. The antenna should move in an elliptical path to resemble the searching behavior of an insect and the antenna (motors) should be stopped immediately after detecting an object. A graph of the antennal movement generated +from a 3D simulation using a polar coordinate system is shown in Fig 7.

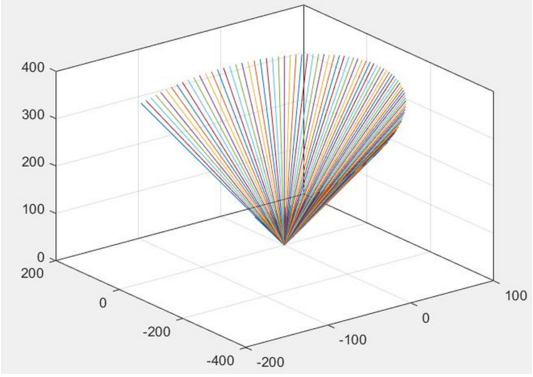

Fig. 7 Animated result for the 3D simulation.

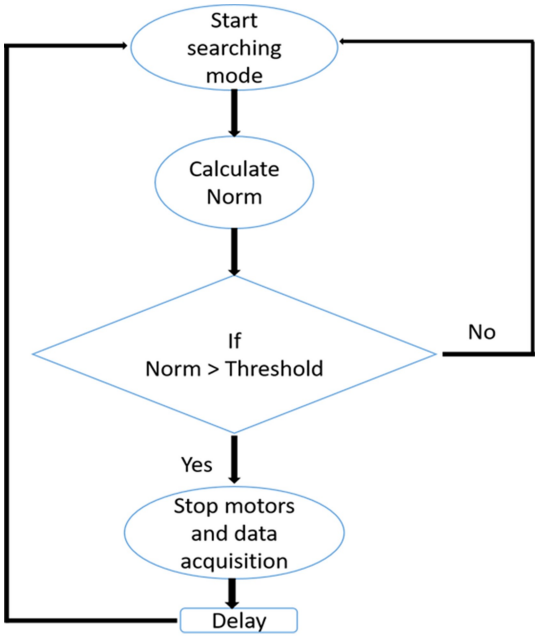

Fig. 8 Block diagram of the control algorithm.

The servo motors, used for the pan-tilt unit should have sufficient torque to bare the 40cm length antenna. Therefore, metal gear MG996R high torque servo motors are used. PCA9685 16 channel servo control unit is connected to the Raspberry pi 3 control board to control the servo motors. Data acquisition setup of the system is shown in Fig 6. The control algorithm of the pan-tilt is based on the block diagram in Fig 8.

4 Discussion

4.1 Results from Signal Processing for Distance Estimation and Material Classification

4.1.1 Distance Estimation

Here a unique feature is found to identify the contact distance from the robot. The feature, frequency of the maximum amplitude frequency component, does not change according to the material and it is dependent only on the contact distance. The resultant plots for the different materials are shown in Fig 9. Although a linear variation behavior is observed for all five materials, a deviation from that linear behavior could be observed at 29.5 cm away from the hinge point of the antenna. After increasing the length of the antenna to 50 cm, a similar deviation could be observed at 39.5cm away from the hinge point. The standard deviation of the sensor readings for both cases are shown in Fig 10, and it is seen that this variation occurs at 80% of the antenna length away from the hinge point. Therefore, 40 cm is selected as the antenna length and 80% from that length is selected for further predictions.

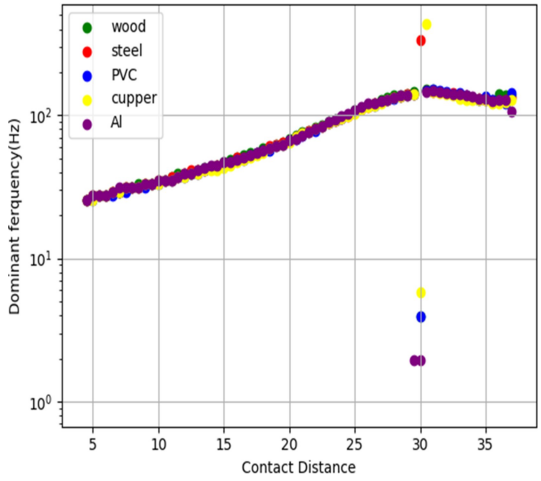

Fig. 9 Variation of the contact distances Vs Log scale of the dominant frequency for the five different materials

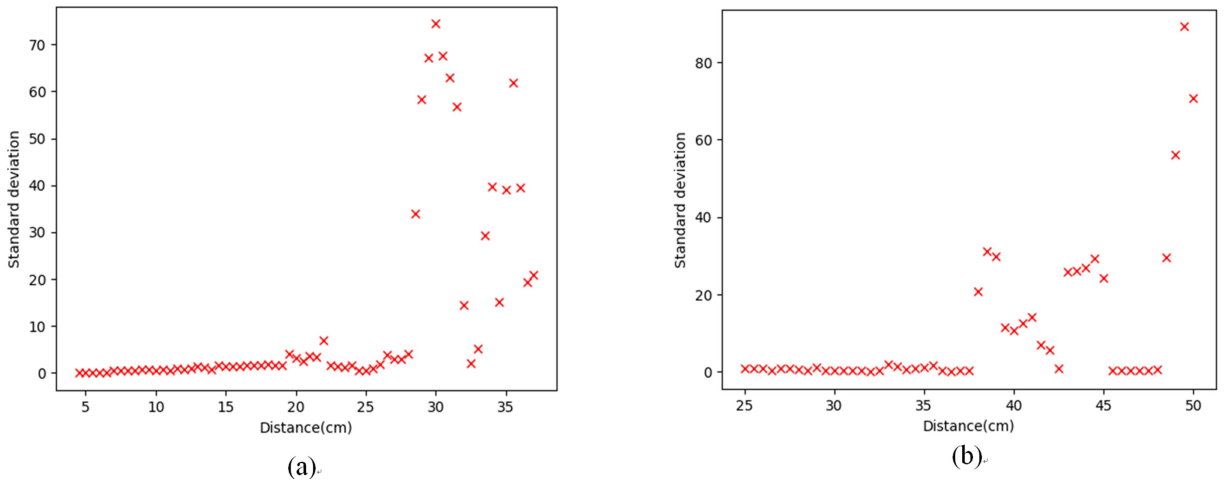

Fig. 10 Variation of the standard deviation Vs contact distance from the hinge point (a) probe length 40 cm (b) probe.

4.1.2 Material Classification

From the figures it is observed that the separation of the materials varies with the frequency band. Therefore, randomly selected frequency bands are used to select the best separable frequency band, and most of the times good classifications have been obtained at the high frequency band.

In the high frequency band, pass band cutoff frequencies are set in the range of 100 Hz- 200 Hz. The time constant varied with the selected band pass cutoff frequencies. After applying several frequency ranges, one range has been selected due to the greater separations it showed than the others. The resultant graphs of the gain and time constant for that particular range are shown in Fig.11. As seen from Fig. 11, a clear variation can be obtained in the 0 - 80% range of the antenna in this frequency band. But here an overlap is observed between PVC and WOOD at 26 cm away from the hinge point. The optimum filter characteristics are given in Table I. As the material separation depends on the frequency band, if the characteristics in Table I are changed, the behavior of the separation will not achieve the optimum separation.

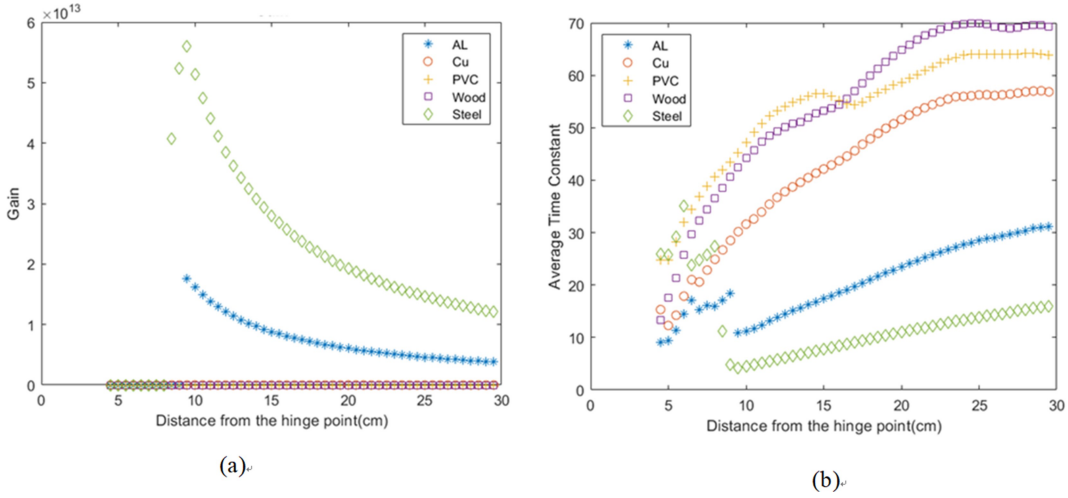

Fig. 11 Variation of the (a) Gain (b) Time constant over the contact distance for five materials.

Table 1 Chebyshev Filter Characteristics.

Sampling Frequency	Fs	1000
Nyquist Frequency	Fn	Fs/2
Normalized Passband	Wp	[60 160]/Fn
Normalized Stopband	Ws	[55 165]/Fn
Passband Ripple (dB)	Rp	1
Stopband Ripple (dB	Rs	30

4.2 Results from ANN

When implementing the ANN, it is trained using the MATLAB toolbox for simulations (Beale, et al., 2010). For the real-time implementation, python 3.0 and tensor flow open source library are used. All the training and testing processes are performed on a computer with Intel (R) 8 Series Chipset processor, 4.00GB RAM, 64-bit operating system, and ×64-based processor. Also, Google cloud platform is used for fast computation and training, in real-time implementation. For classification and distance estimation tasks, two different kinds of ANN models have been tested. The training, testing and validation datasets are created by the magnitude values of the FFT frequency spectrum (256 components). The dataset is created for all five materials by changing the contact distance along the antenna in 5 mm steps, and for each contact point, 25 samples are taken. The full dataset is split as 70% for training, and 15% each for testing and validation. The full dataset is normalized (by dividing by the maximum magnitude of the frequency component), and no dimension reduction method is used. For the material classification, different Neural network topologies have been tested to find the optimum one. The training algorithms, activation functions, the number of hidden layers and the number of neurons per hidden layer have been changed, and the model has been optimized in order to realize a model with high performance. The optimum result is generated by a single hidden layer with 53 neurons. The training algorithm is gradient descent, and the activation function is tanh. The overall confusion plot for the optimum model in the material classification task is shown in Fig.12.

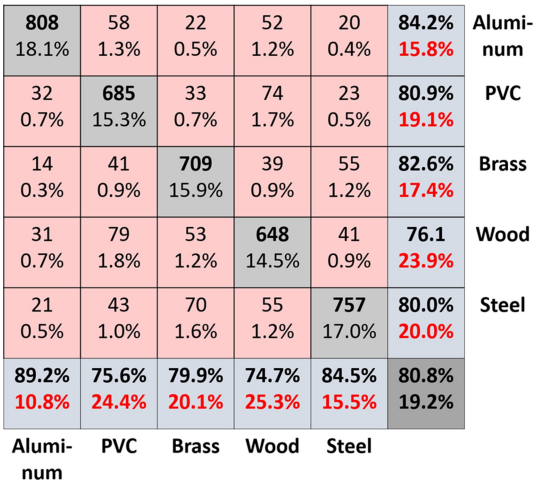

Fig. 12 Confusion matrix.

The diagonal elements of the confusion plot give the correctly classified number of material for the entire training and testing dataset. The average overall accuracy for material classification is 80.8%. The percentage value shown in each cell of the matrix is the detected number of samples from the full dataset. The proposed material classification method is extended to contact distance estimation from the hinge point. A regression type neural network is used in order to predict the contact distance. To train the regression model, the same dataset as in the material classification task, is used. From the signal processing observation, it is concluded that towards the tip of the antenna, the nonlinear behavior becomes dominant. Therefore in order to train the regression model, only the linear behavior dataset (approximately 80% from the full antenna length) is used. The best result for the distance prediction is provided by 2 hidden layers with 20 neurons per layer. The training algorithm is gradient descent and tanh function is the activation function. Fig.13 shows the optimum model performance.

Earlier studies show that the nonlinear behavior of the distance measurement towards the tip of the antenna is a significant issue. Therefore, those studies limited up to 75% (Volker, no date) of the con-

tact distance from the hinge point. In the present study, this behavior is modeled along the antenna. Therefore in order to predict the contact distance in the nonlinear region, a special neural network was trained, providing better performances. Key features of this network are that the dataset is normalized by the min-max normalization method, and the use of a prepossessing stage before feeding to the neural network. In order to remove power line hum and noise, a second order elliptical filter is applied to the dataset. The performance of the filter is improved through experimenting. The optimum filter characteristics are shown in Table 2.

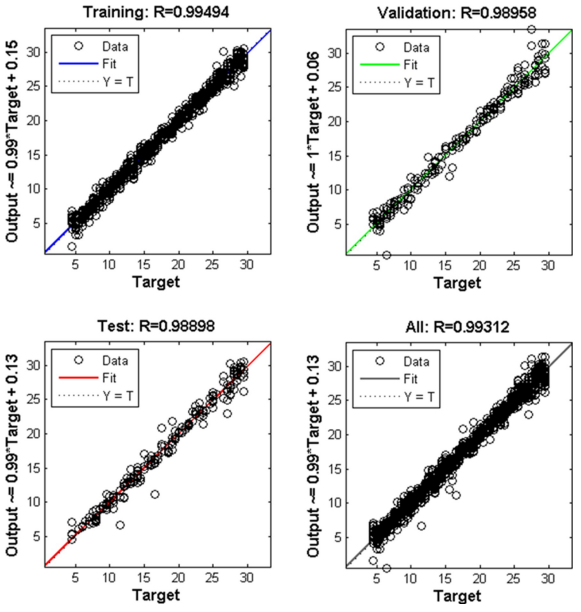

Fig. 13 Optimum model performances.

Table 2 Elliptical Filter Characteristics.

Fs	1000	Sampling Frequency
Fn	Fs/2	Nyquist Frequency
Wp	[52 325]/Fn	Normalized Passband
Ws	[48 330]/Fn	Normalized Stopband
Rp	1	Passband Ripple (dB)
Rs	45	Stopband Ripple (dB

The normalized dataset is split into training, testing, and validation sets at percentage values 70%, 15%, and 15%, respectively. Several models are trained and the optimum model is achieved by hyper parameter tuning. The specifications of the optimum model are the following. Scaled conjugate gradient algorithm is used as the training algorithm, and a single hidden layer consisting 9 hidden neurons is used. Rectified linear unit (ReLU) is selected as the activation function of the model. Fig. 14 shows the performance of the optimum model.

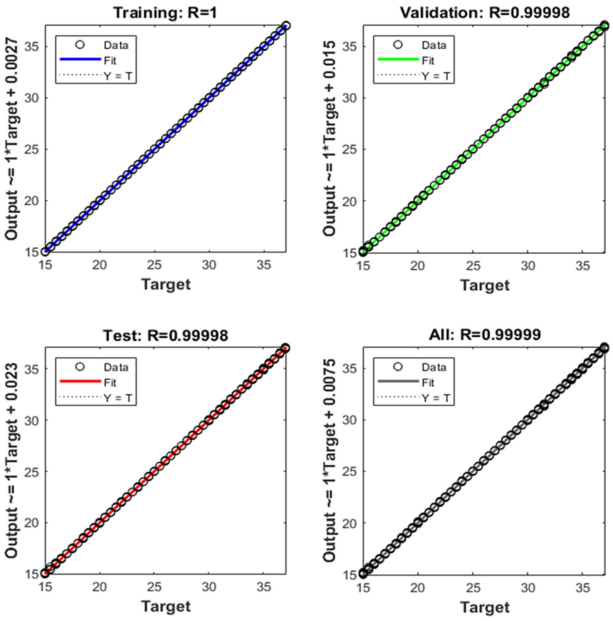

Fig. 14 Performance of the optimum model.

4.3 Results from SVM

Several recent studies have shown that SVM can provide a better performance in classification than with other classifiers (Byvatov, et al., 2003; Singla, et al., 2011). A key factor in using SVM in the present work is that it decides the decision boundary of the classes in order to maximize the gap between classes. For a fair comparison, the training and testing processes of SVM are done using the same dataset that is used for the classification by ANN. In SVM, for a single sample of data, there are 256 (magnitude of frequency components) features as in ANN. Initially, in training the SVM model, a linear SVM was used, which was unable to obtain a well performing model. Subsequently, the kernel was changed in order to improve the performance on the

dataset (nonlinearly separable data).

A different approach is used to form the linear SVM by solving the dual of the optimization problem. The dual for the linear SVM problem is given by,

$$max \sum_{i=1}^{n} b_i - \frac{1}{2} \sum_{i=1}^{n} \sum_{j=1}^{n} y_i b_i (x_i . x_j) y_j b_j \quad (5)$$

where,

$$\sum_{i=1}^{n} b_i y_i = 0 and 0 \leq b_i \leq \frac{1}{2ny} \quad (6)$$

Here the b vector is a variable and it will only have the values +1 and -1. The input data points are visualized in x_i and the targets are in y_i. The mentioned kernel is the $x_i . x_j$ and it is a linear kernel. Rather than using the dot product, a more complicated function is introduced. Specifically, the Gaussian kernel (radian basis kernel) is used, as given by,

$$k(x_i, x_j) = exp(-\gamma \|x_i - x_j\|^2) \quad (7)$$

886 217	1 2	0 1	1 1	1 1	Al
3 0	966 238	0 0	1 0	0 1	Brass
0 0	1 0	980 272	3 0	0 0	PVC
2 2	0 2	0 0	1020 238	1 0	Steel
1 0	0 0	1 0	1 0	931 225	Wood
Al	Brass	PVC	Steel	Wood	99.7% 99.2%

Fig. 15 Confusion plot for the optimum SVM model.

Here, $\|x_i - x_j\|^2$ is the square of the Euclidean distance between the feature vectors and the Gamma value is changed accordingly (Nanda, et al., 2018; Nahar, et al., 2007). The optimum model was obtained for 2.0 gamma values and with 50 iterations in training the model. In training the SVM model we use one vs all strategy, and the gradient descent optimizer as the training algorithm. The batch size is selected as 6000 samples and 80% of it is used as the training dataset, and the remaining 20% as the testing dataset. Fig.15 shows the confusion plot in material classification using SVM. Here white color refers to training results and red color refers to testing results. The accuracy for training and testing is 99.7% and 99.2%, respectively. The SVM method gives a better performance than with the signal processing technique and artificial neural network in accuracy as well as in computational cost.

4.4 Experimental Verification of Vibration Mode Change

The dominant vibration modes are obtained from the numerical solution of the mathematical model. When contact point is moved from the hinge point to the tip, the shape of the dominant vibration mode also varies. Therefore, a change in the dominant vibration mode should happen as well. In Fig. 16, three zones can be identified in the frequency variation. Initially, it has a very slight variation with a llow gradient. But when moving towards the antenna tip, the gradient of the linear variation increases. As the contact object is very close to the hinge point, the beam element between the hinge point and the contact point shows a high stiffness and the rest of the beam element behaves like a cantilever (see Fig.17(a)). But when the contact point moves towards the antenna tip, as in Fig.17 (c), the cantilever action becomes stiffer. Therefore the antenna element between the contact point and the hinge point becomes more flexible and again a slight variation is observed but it is different from the initial variation, as shown in the Fig 16 Zone 3. When the contact distance is between these two cases, a transition of the modes is observed, as in Fig 17 (b). The vibration mode is changed in the range of Zone 2 (see Fig 16). Hence, at the 80% of the total antenna length, the mode of vibration is entirely changed. This change in mode of vibration is the main reason for the deviation from the linear variation, obtained in the signal processing algorithm.

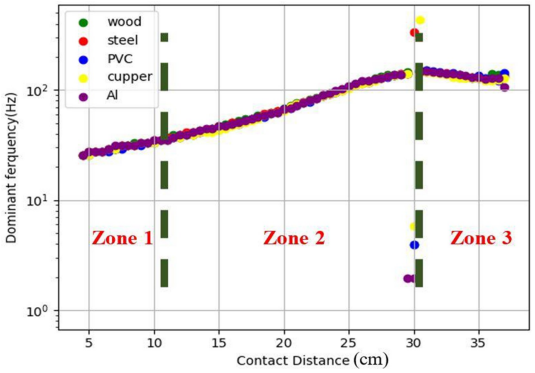

Fig. 16 Variation of the dominant frequency vs contact distance according to the zones.

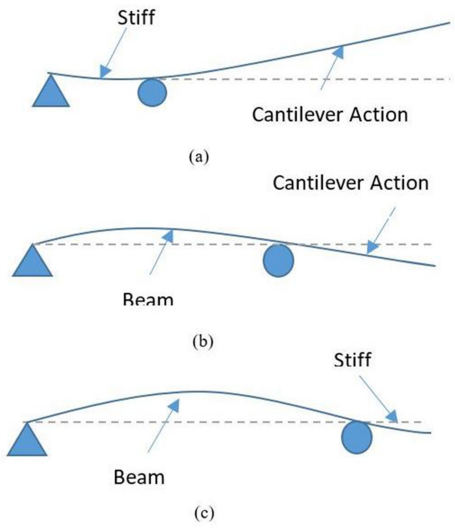

Fig. 17 Modes of vibration.

In signal processing a spectrum shows the frequency content of an entire signal. It is a 1-dimensional function of amplitude versus frequency whereas a spectrogram shows how the frequency content of a signal changes over time. It is a graph with two dimensions: frequency (vertical axis) and time (horizontal axis). The third dimension is the amplitude of a particular frequency at a particular time, which is represented by the intensity of each point in the image/graph. Spectrograms are constructed by breaking the time domain data into a series of chunks and taking the FFT and then overlapping these FFTs with one another so that one can visualize how both amplitude and frequency of the signal changes with time. Spectrograms are constructed for experimentally obtained vibration signals (norm) at different contact lengths.

These spectrograms of vibration signals are used to verify the numerical solutions of the mathematical model, i. e., the existence of multiple vibration modes when a contact happen towards the tip of the antennal probe. The results, obtained using wavelet spectrogram for the $0.25L$, $0.5L$, $0.75L$, $0.8L$ and $0.9L$ of the antenna length are discussed now. According to the results obtained from the mathematical model, a total vibration mode change occurs at $0.8L$. Fig.18 shows the spectrogram of the vibration signal at $0.25L$ and $0.5L$. Both of these points are laid on the linear region of Fig 16. The dc component is laid at 0.0 of the frequency axis. Even though it has some powerful frequency components in the beginning, the most powerful frequency component for the $0.25L$ is between 0.05-0.1 in the normalized frequency, and it is between 0.1-0.15 for the $0.5L$. Both these frequency components remain powerful during more than 300 samples of the signal and the remaining components that occur in the beginning do not appear. This is a cantilever behavior in the antenna beam as shown in Fig.17 (c). In this mode the antenna tip shows a more flexible vibration pattern than others. Because of that the dominant frequency component lasts longer than in the other cases.

When analyzing the vibration signals at $0.75L$, $0.8L$ and $0.9L$, the behavior of the spectrogram is entirely different from the previous cases. Three spectrograms for the signals at lengths $0.75L$, $0.8L$ and $0.9L$ are shown in Fig.19 (c), (d) and (e), respectively. Although all three cases have a powerful frequency component in the beginning (most yellow colored one), they disappear with time. This is because the vibration mode is in Zone 3 of Fig.16 and because of the cantilever action becomes stiffer, these modes quickly disappear. Now the vibration pattern is similar to that in Fig.17 (c). This verifies the existence of multiple vibration modes when a contact happens towards the distal end of the antennal probe. In fact, it is as expected by the numerical solutions of vibration

analysis of the model of the antenna.

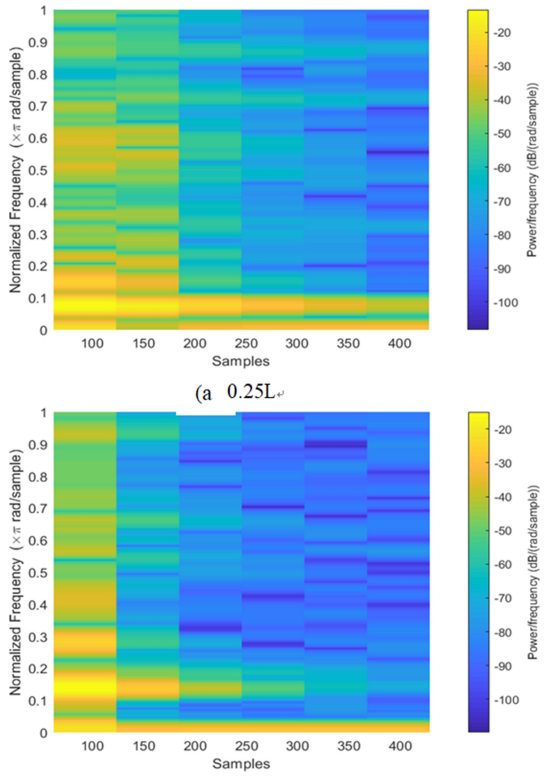

Fig. 18 Spectrogram of the norm of the vibration signal at (a) 0.25 *L* (b) 0.5 *L*.

Moreover, many powerful frequency components can be obtained in the beginning than in the cases presented in Fig 18. That means, in the beginning there are many vibration modes and most of them disappear after 100 samples, and the rest of them also have very low power compared to the DC component. Fig.19(e) has more powerful frequency components in the beginning than for all other cases, and also, they all vanish quickly. Therefore, it is unable to identify a good dominant frequency component to carry the properties of the entire vibration signal. More significantly, the 0.75 *L* and the 0.8 *L* cases are in the beginning of the deviation from the linear behavior in Fig.16. The 0.9 *L* case is observed in the deviated region. By applying an adaptive band pass frequency tracking filter, the most suitable frequency component may be found to represent the dominant frequency. With that it will be able to estimate the distance in the full range of the antenna.

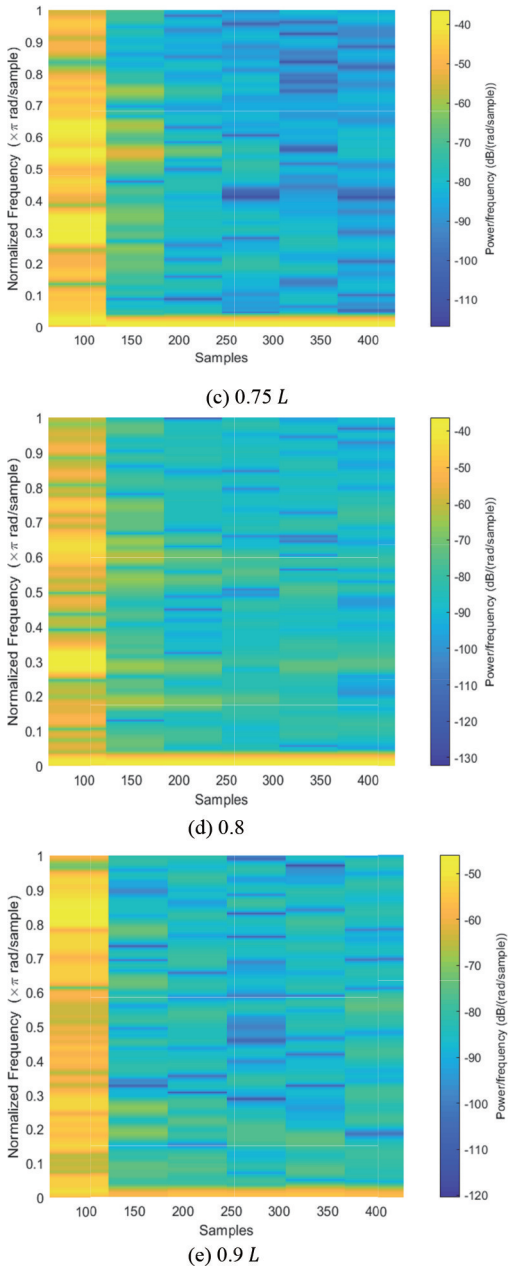

Fig. 19 Spectrogram of the norm of the vibration signal at (c) 0.75 *L*, (d) 0.8 *L* (e) 0.9 *L*.

5 Conclusion

This paper presented a bionic active tactile sensor inspired by the antenna of the stick insect, which was capable of object detection, material classification, and object localization. Since the existing methods were unable to predict the contact distance along the full length of the antenna, the reason for this scenario was analyzed. Initially possible causes

for the abnormal behavior were identified using mathematical analysis based on the Euler-Bernoulli beam element model. Form the mathematical analysis, vibration mode change in the antenna beam was identified as the reason for the abnormal behavior of the results. The results obtained from mathematical analysis were verified using experimental results obtained from spectrogram analysis, which was in good agreement with the theoretical analysis. As the theoretical results fully agreed with the experimental results, it was concluded the mode of vibration change was the reason behind the abnormal behavior of the results. A suitable method to use the full range of the antenna probe was suggested. As an approach for Achieving better performance in material classification, an ANN model was developed that used preprocessing through signal processing techniques. For the material classification task, it introduced SVM, which provided better accuracy than with existing signal processing techniques and ANN model. While the overall accuracy obtained from the ANN was 80.8%, better than 99% accuracy was obtained through the SVM model for the same data set in the classification process at a lower computational cost. Hence, the SVM was selected to classify the materials, as it provided high accuracy at a low computational cost.

References

[1] Beale, M. H., Hagan, M. T. & Dimuth, H. B., 2010. *Neural Network Toolbox TM 7 User´s Guide.* s. l.:The Mathworks Inc.

[2] Bisgin, H. et al., 2018. Comparing SVM and ANN based Machine Learning Methods for Species Identification of Food Contaminating Beetles. *Scientific Reports*, 8(6532).

[3] Byvatov, E., Fechner, U. & Sadowski, J. S. G., 2003. Comparison of Support Vector Machine and Artificial Neural Network Systems for Drug/Nondrug Classification. *J. Chem. Inf. Comput. Sci.*, 43(6), pp. 1882-1889.

[4] De Silva, C.W., *Vibration—Fundamentals and Practice*, 2nd Edition, Taylor & Francis/CRC Press, Boca Raton, FL, 2007.

[5] De Silva, C.W., *SENSOR SYSTEMS—Fundamentals and Applications*, Taylor & Francis/CRC Press, Boca Raton, FL, 2017.

[6] Dürr, V. et al., 2007. Bionic Tactile Sensor for Near-Range Search, Localisation and Material Classification. In: K. Berns & T. Luksch, eds. *Autonome Mobile Systeme* 2007. *Informatik aktuell.*. Kaiserslautern: Springer, Berlin, Heidelberg, pp. 240-246.

[7] ElectronicWings, 2018. *MPU6050 (Accelerometer+Gyroscope) Interfacing with Raspberry Pi.* [Online] Available at: http://www.electronicwings.com/raspberry-pi/mpu6050-accelerometergyroscope-interfacing-with-raspberry-pi[Accessed 17 March 2018].

[8] Hamioud, S. & Khalfallah, S., 2016. Free-vibration of Bernoulli-Euler beam using the spectral element method. 10(3-4), pp. 106-112.

[9] Harischandra, N. & Dürr, V., 2012. *A Forward Model for Active Tactile Sensor Using Echo State Networks*. Magdeburg, IEEE International Symposium on Robotic and Sensors Environments (ROSE), pp. 103-108.

[10] Hoinville, T., Harischandra, N., Krause, A. F. & Dürr, V., 2014. *Insect-Inspired Tactile Contour Sampling Using Vibration-Based Robotic Antennae.* s.l., Springer, Cham, pp. 118-129.

[11] Karray, F.O. and de Silva, C.W., *Soft Computing and Intelligent Systems Design—Theory, Tools, and Applications*, Addison Wesley, New York, NY, 2004.

[12] Krause, A. F., Hoinville, T., Harischandra, N. & Dürr, V., 2014. *Contour-Net, a model for tactile contour tracing and shape recognition.* Loire Valley, Springer, pp. 92-101.

[13] Nahar, J., Ali, S. & Chen, Y. P., 2007. Microarray data classification using automatic SVM kernel selection. 26 10, 707-12 ..*DNA and cell biology*, 26(10), pp. 707-712.

[14] Nanda, M. A., Seminar, K. B., Nandika, D. & Maddu, A., 2018. A Comparison Study of Kernel Functions in the Support Vector Machine and Its Application for Termite Detection. *Information*, 9(5).

[15] Patanè, L. et al., 2012. An insect-inspired bionic sensor for tactile localization and material classification with state-dependent modulation. *Front. Neurorobot.*, 6(8).

[16] Ren, J., 2012. ANN vs. SVM: Which one performs better in classification of MCCs in mammogram imaging. *Knowledge-Based Systems*, Volume 26, pp. 144-153.

[17] Sayed, M. A., 2015. *Properties Of Acrylic Fibre.* [Online] Available at: https://textileapex.blogspot.com/2015/03/properties-of-acrylic-fibre. html [Accessed 24 March 2018].

[18] Singla, R., Chambayil, B., Khosla, A. & Santosh, J., 2011. Comparison of SVM and ANN for classification of eye events in EEG. *Biomedical Science and Engineering*, Volume 4, pp. 62-69.